Journal of Highway and Transportation Research and Development
2024, 18(4): 90−102

Research Article
ISSN 2095−6215
DOI: 10.26599/HTRD.2024.9480038

Status assessment and management strategy of a large bridge based on massive real time data

Feng Zhou[1*], Zhihao Cui[2**]

1. *CCCC-TDC Environmental Engineering Co., Ltd., Tianjin 300461, China*;
2. *HCIG Communications Investment Co., Ltd., Shijiazhuang, Hebei 050051, China*

Abstract: This study aims to enhance the understanding of the state of large-scale bridge structures by accurately analyzing the structural changes of bridges through extensive real-time monitoring data. By conducting a comparative analysis of field load test data and simulation calculations of linear models, this research seeks to provide a precise assessment of structural indices, identify potential risks, and develop appropriate preventive measures. Using a domestic long-span suspension bridge as a case study, the bridge beam is conceptualized as a multi-degree-of-freedom structure, allowing for the application of linear structural vibration mode decomposition methods. During the on-site load testing, a structural health monitoring system is employed to collect real-time data, which facilitates the calculation of deflection and strain values for each control section under static load conditions. Additionally, the frequency response function, unit pulse response function, and covariance-related functions are utilized to derive the modal parameters of the structure during dynamic load testing. The health monitoring system's measurements of strain, deflection, and modal parameters are then compared with the analytical results from the tests, while also verifying the operational integrity of the monitoring system. By referencing the assessment methodology for site load tests, this research analyzes the data mining from health monitoring systems to evaluate the bridge's load-bearing capacity during testing, as well as for subsequent evaluations of the bridge's structural health and operational status. The experimental findings demonstrate that the load testing equipment and health monitoring system effectively capture significant vehicle loading and unloading events. Furthermore, the analysis of the acquired vibration data yields reliable modal parameters, with deflection calibration coefficients and relative residual coefficients meeting established criteria. The calculated frequencies are found to exceed the theoretically predicted values, indicating that the global stiffness of the structure aligns with design specifications and that the mechanical properties comply with regulatory standards. This reflects the feasibility and effectiveness of the monitoring-based evaluation index system and methodology employed in this study.

Keywords: bridge engineering; large-scale bridge; structural health monitoring system; massive real-time data; load test; status assessment.

1 Introduction

In recent decades, with the rapid development of economic level, more and more large-span bridges have been built in China, such as the Hong Kong-Zhuhai-Macao Bridge (HZMB), which is the longest cross-sea bridge in the world, has been completed and opened to traffic. The stability of bridge structure is the safety guarantee for people's life and property, however, due to the rapid growth of vehicle ownership and overloading phenomenon, making some of the bridges in service during the vehicle load has exceeded its design load. Such a result inevitably leads to major safety accidents during the service period of the bridge, such as the Wuxi viaduct rollover accident that occurred in 2019. Sudden collapses, ruptures and other major accidents of various types of bridges are bound to cause major casualties and social impact, which requires that we must pay attention

Received: 16 August 2024; **Revised:** 10 October 2024; **Accepted:** 30 October 2024

[*] *E-mail address*: 94175213@qq.com
[**] *Corresponding author*: 542389337@qq.com

to the safety of all types of transportation facilities in real time and prevent them in a timely manner. Therefore, it is of great significance to carry out real-time monitoring, analysis and evaluation for the structural state of major transportation facilities, timely discover the structural diseases, and assess the degree of its impact on the main body of the structure, predict the degradation rate and remaining life of the structure and timely repair to ensure the safety of transportation facilities[1].

Structural health monitoring of bridge can sense, monitor, identify, evaluate and warn the structural load and environmental action, structural correspondence, structural performance, structural condition and safety level in real time, which is an effective method and technology to guarantee the safety of the structure in whole-life service[2]. The health monitoring system of bridge mainly includes the installation and deployment of sensors on the main girder and other structures, real-time data acquisition system, and system analysis of bridge deformation and load response[3-5]. At present, a number of scholars have carried out related research. As early as 2012, Chao Wang et al.[6] conducted fatigue assessment of steel box girders using the measured stress of health monitoring system, based on the linear cumulative damage criterion and the fatigue strength curves of each connecting part of the steel box girders, fatigue damage assessment of the main girders, and real-time updating of the assessment results based on the change of the traffic condition. 2016 Xu et al.[7] For the first time, a distributed fiber-optic sensing system was deployed on the main girder of a large-span suspension bridge, and the deformation characteristics of the main girder of the bridge were measured in a fully distributed manner during the load test of the suspension bridge, and the condition of the bridge was assessed. 2017 Wei et al.[8] A quasi-distributed fiber-optic grating sensing technology was used to construct an identification system for the cracks of the main girders of the suspension bridge, which was able to identify the cracks of the main girders efficiently by identifying the dynamic vehicular loads on the bridge. 2019 Chuanxi Li et al.[9] In order to study the fatigue characteristics of the parent material at the curved cutout of the steel box girder diaphragm under the effect of vehicular load, the Foshan Pingsheng Bridge is taken as the background project, and the service state of the bridge is effectively evaluated based on the monitoring data of the dynamic weighing system (WIM).

The combination of bridge load test and bridge structural health monitoring system can effectively understand the performance of the bridge structure during service and its working condition under load, which is substantial to know for the reconstruction or overhaul and reinforcement of important bridges[10-12]. Load test of bridge structure generally consists of static load test and dynamic load test. Static load test test bridge structure in the test load under the action of control cut-off and the strain, displacement. The dynamic load test tests the response of the bridge under dynamic loading and analyzes the modal parameters such as frequency and vibration pattern of the bridge[13-14]. Evaluation of bridge load carrying capacity based on strain, displacement, and modal parameters[15]. Currently, the design and implementation of bridge load tests have a very complete system, and the test results have been fully verified.

This paper firstly analyzes the damage identification method of the bridge structural health monitoring system, and establishes a health monitoring system for the main girder structural system of a suspension bridge, which includes quasi-distributed fiber-optic grating dynamic strain sensing, monitoring of bridge deflection and deformation based on the GPS technology, and identification of structural modes. The structural health monitoring system data during the on-site load test and the deformation characteristics of the main girder under the corresponding load position are analyzed. The health monitoring data were analyzed and mined to evaluate the load carrying capacity of the bridge during the load test with reference to the evaluation method of the field load test. The research method can be used as a reference for subsequent evaluation of the structural health monitoring system and the operation of the bridge.

2 Principles of bridge structural damage identification

Damage identification and modal modification in structural health monitoring are often based on structural parameters, therefore, the analysis of structural modes is an important part of structural health diagnosis. The theory of structural health diagnosis is to analyze the monitoring data, firstly get the covariance of the frequency response function or unit impulse response function or correlation function of the structure, and then identify the modal state of the structure through the relationship between the frequency response function and the modal parameters of the structure, and ultimately identify the damage of the structure[16].

For the large-span suspension bridge girders can be regarded as a structure with multiple degrees of freedom, and its differential equations of motion are:

$$\boldsymbol{M}\ddot{x}+\boldsymbol{C}\dot{x}+\boldsymbol{K}x=f \tag{1}$$

where, $\boldsymbol{M}$ is the mass of the mechanism; $\boldsymbol{C}$ is the damping of the structure; $\boldsymbol{K}$ is the stiffness matrix of the structure; x is the displacement vector of the structure; f is the load vector of the structure.

Applying Rasch and Fourier transforms to Equation (1) yields

$$\left(\boldsymbol{M}s^2+\boldsymbol{C}s+\boldsymbol{K}\right)x(s)=f(s), \tag{2}$$

$$\left(\boldsymbol{K}-\omega^2\boldsymbol{M}+\mathrm{j}\omega\boldsymbol{C}\right)x(\omega)=f(\omega). \tag{3}$$

From the structural dynamics, it can be obtained that the response of the linear structure can be solved by the vibration mode decomposition method, then the i point response can be expressed as:

$$x_i(\omega)=\sum_{r=1}^{N}\varphi_{ir}q_r(\omega), \tag{4}$$

where, φ_{ir} are the vibration coefficients of the i points at the rth order modes; $q_r(\omega)$ are the generalized coordinates of the r order modes.

The r order modal vector or mode vector is

$$\boldsymbol{\varphi}_r=\{\varphi_{1r},\varphi_{2r},\cdots,\varphi_{Nr}\}^{\mathrm{T}} \tag{5}$$

The matrix consisting of the modal vectors of each order is

$$\boldsymbol{\Phi}=\{\varphi_1,\varphi_2,\cdots,\varphi_N\}^{\mathrm{T}} \tag{6}$$

The displacement vector of the structure is obtained from Equations (4) and (6) as

$$x(\omega)=\boldsymbol{\Phi}q \tag{7}$$

Bringing Equation (7) into Equation (2) yields

$$\left(\boldsymbol{K}-\omega^2\boldsymbol{M}+\mathrm{j}\omega\boldsymbol{C}\right)\boldsymbol{\Phi}q=f(\omega) \tag{8}$$

For multi-degree-of-freedom structure, when the structure is undamped or the damping ratio is proportional damping, each degree of freedom of the structure are vibrating in the same phase or anti-phase, the vibration form of the structure remains unchanged and is expressed in the form of standing wave[17]; when the structure is damped by non-proportional damping, the modal parameters of the structure are generally complex, and the structure is vibrating in different phases at this time, and the vibration shape of the structure can not be maintained and is expressed in the form of traveling wave. The shape of structural vibration cannot be maintained, and it is in the form of traveling wave. Assuming that the damping ratio of the beams of this large-span suspension bridge is proportional damping, the generalized modal coordinates of the r order are as follows

$$q_r=\frac{f_r^*}{\boldsymbol{K}_r^*-\omega^2\boldsymbol{M}_r^*+\mathrm{j}\omega\boldsymbol{C}_r^*}. \tag{9}$$

The r order generalized modal loads are

$$f_r^*=\varphi_{pr}f_p(\omega). \tag{10}$$

Bringing Equations (9) and (10) into Equation (4), the displacement response at point i of the structure is obtained as

$$x_i(\omega)=\sum_{r=1}^{N}\frac{\varphi_{ir}\varphi_{pr}f_p(\omega)}{\boldsymbol{K}_r^*-\omega^2m\boldsymbol{M}_r^*+\mathrm{j}\omega\boldsymbol{C}_r^*}. \tag{11}$$

The frequency response function between the response of the structure at the measurement point l and the load p is

$$H_{lp}(\omega)=\frac{x_i(\omega)}{f_p(\omega)}=\sum_{r=1}^{N}\frac{\varphi_{lr}\varphi_{pr}}{\boldsymbol{K}_r^*-\omega^2\boldsymbol{M}_r^*+\mathrm{j}\omega\boldsymbol{C}_r^*}. \tag{12}$$

The frequency response function $H_{lp}(\omega)$ refers to the complex response at point l produced by applying one unit load at point p of load. From Equation (12), it can be obtained that the frequency response function is not related to the magnitude and type of load. And the frequency response function of the structure is the superposition of the frequency response function of each individual mode, but in most of the actual structures, the main modes involved in structural vibration are the first few or a dozen modes, and other higher-order modes contribute less to the structural vibration or even don't appear, so the higher-order modes can be truncated in the analysis. In order to minimize the effect of truncated modes, the residual flexibility is often used to replace these truncated modal responses. At this point the frequency response function can be written as

$$H_{lp}(\omega) = \sum_{r=1}^{N_c} \frac{1}{K_{er}\left[\left(1-\overline{\omega}_r^2\right)+j2\zeta_r\overline{\omega}_r\right]} + H_c. \qquad (13)$$

where, $N_c(<N)$ is the number of truncated modes, which should be greater than twice the analyzed modes, and H_c is the residual softness, which can be regarded as a frequency-independent constant or a linear function of the frequency ω[18].

The Fourier transform of Equation (12) yields the impulse response function as

$$H_{lp}(t) = \sum_{r=1}^{N} \frac{\varphi_{lr}\varphi_{pr}}{M_r^*\omega_r} e^{-\zeta\omega_0 t} \sin(\omega_r t). \qquad (14)$$

Through the above theoretical analysis, the structural modal parameters can be solved, so that the damage of the bridge can be effectively identified.

3 Overview of load test

3.1 Overview of the bridge

This type of bridge is a large-span double-tower double-span suspension bridge with a main span length of 1 688 m and a span arrangement of (658 + 1 688 + 522) m, of which the length of steel box girder is 548 m+ 1 688 m (Figure 1). The vector span ratio is 1:9.5, the center spacing of main cable is 42.1 m in transverse direction, and the standard spacing of sling is 12.8 m in downward direction. The bridge cross-section arrangement is as follows: 0.5 m guardrail +18.75 m carriageway +0.75 m guardrail +0.5 m central median +18.75 m carriageway +0.5 m guardrail, the detailed dimensions are shown in the bridge layout plan and standard cross-section plan.

3.2 Static load test

Field load test mainly includes static load test and dynamic load test. The dynamic load test is divided into pulsation test and running and jumping test. The static load test tests the strain and displacement of the control section of the bridge structure under the test load. Based on the strain and displacement, the load carrying capacity of the bridge is evaluated[19].

3.2.1 Control section and test conditions for static load test

The static load test control section is shown in Figure 2. The main beam is divided into 10 test sections in the figure. They are defined as A-A, B-B, C-C, D-D, E-E, F-F, G-G, H-H, I-I, and J-J, respectively. The specific part of A-A test section is the middle of the side span, and the key indexes of the test are the bending moment and deflection of the side span; the specific part of B-B test section is the tower-beam junction position on the A side, and the key indexes of the test are the bending moment of the main beam; the specific part of C-C test section is the top of the tower on the A side, and the key indexes of the test are the tower top deviation; the specific part of D-D test section is the distance of the main tower from the deck of the A side to above 2 m. The key indexes of the test are the cable-stayed tower, and the key indexes

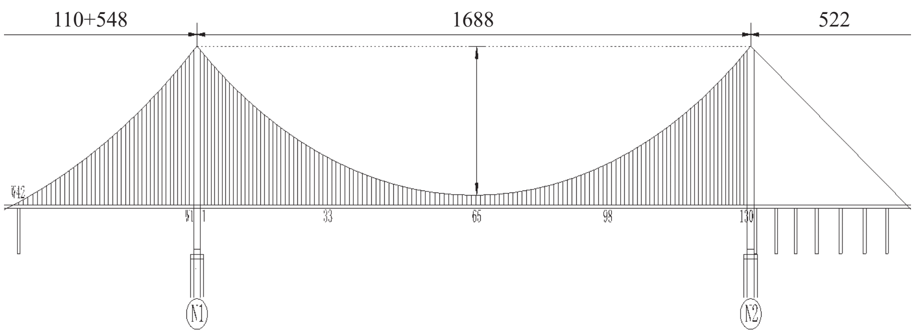

Fig. 1 Sling numbering diagram (unit: m)

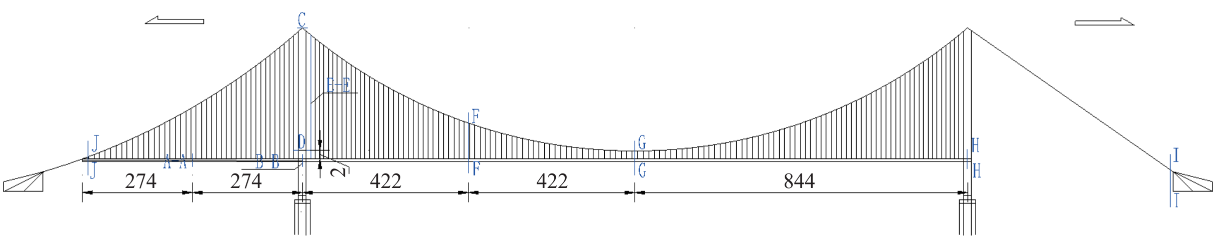

Fig. 2 Location of main test sections (unit: m)

of the test are the cable-stayed tower and the cable-stayed tower. The specific part of D-D test section is 2 m above the bridge deck from the main tower on the A side, and the key index of the test is the bending moment of the tower; E-E test section is the specific part of the longest sling of the tower on the A side, and the key index of the test is the increment of the cable force; F-F test section is the specific part of the tower close to the *L*/4 position on the A side, and the key index of the test is the vertical displacement of the main girder; G-G test section is the specific part of the span, and the key index of the test is the bending moment of the span, and deflection of the main girder; H The specific part of H test section is the beam end of B side, and the key index of the test is the longitudinal displacement of the beam end; the specific part of I-I test section is the anchor position of the main cable of B side, and the key index of the test is the tension of the cable strand across the anchor; the specific part of J-J test section is the limiting sling of B side, and the key index of the test is the increment of the cable force.

The static load test is divided into five loading test conditions, and the specific information of each test condition is shown in Table 1.

3.2.2 Arrangement of measuring points for static load test

The deflection measurement of static load test mainly uses total station and electronic level, of which the arrangement of total station in the longitudinal direction on the bridge is shown in Figure 3. The layout in the cross-section is shown in Figure 4 and Figure 5, and the layout of the electronic level is shown in Figure 6.

Electronic level measuring point of key section of main girder: the main object is 2 measuring points in the middle of cross section of key section (side span center, middle span *L*/4, middle span center), aiming at using electronic level measurement in the case that connecting pipe can not detect the relative deformation of the key section in transverse direction.

The main tower, the main cable deformation measurement points mainly include: the main cable deformation using $4^{\#}$ station (set up in the middle of the span of the

Table 1 List of test conditions

Working condition	Control section	Control item	Loading mode
Working condition 1	C-C, D-D, G-G, I-I, J-J	Mid-span bending moment and deflection, A-side tower top deflection, tower root bending moment, main cable anchor span tension, limit sling tension	Bias load, symmetrical loading
Working condition 2	F-F	Maximum deflection and bending moment of A-side L/4 position section	Bias load, symmetric loading
Working condition 3	B-B, E-E	Maximum negative bending moment and maximum sling force at the tower-beam junction on A-side	Bias load, symmetrical loading
Working condition 4	H-H	Maximum longitudinal drift of A-side beam end	Bias load, symmetrical loading
Working condition 5	A-A	Maximum deflection and bending moment at mid-span section of side span	Bias load, symmetric loading

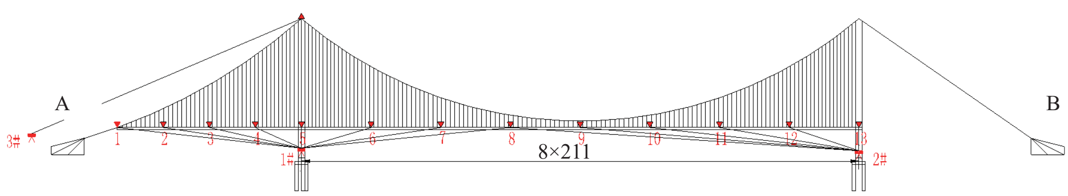

Fig. 3 Longitudinal arrangement of deflection measurement points on the bridge (unit: m)

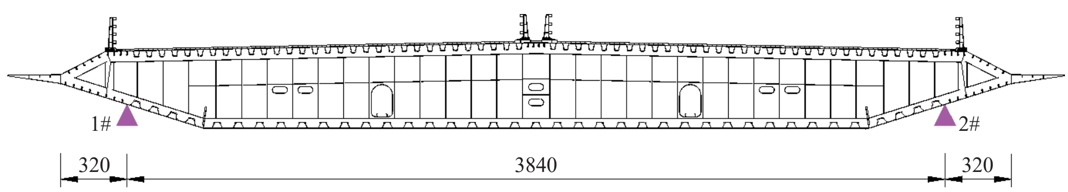

Fig. 4 Horizontal layout of deflection measurement points of general section (unit: cm)

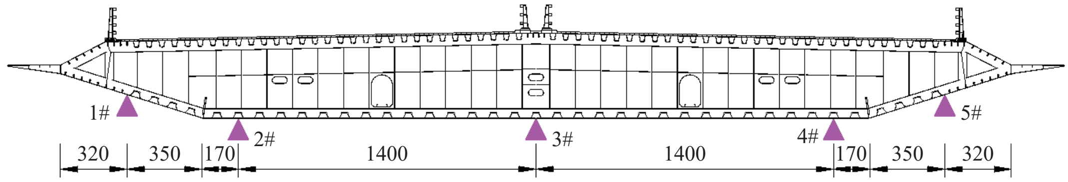

Fig. 5 Horizontal layout of deflection measurement points of control section (side span center, middle span L/4, middle span center) (unit: cm)

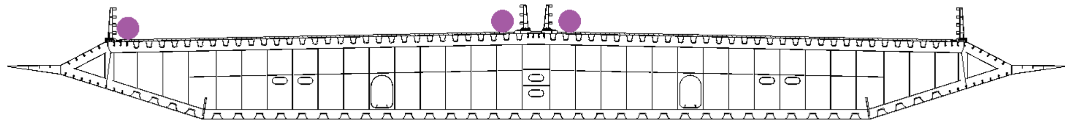

Fig. 6 Arrangement of measuring points of electronic level meter

left width of the bridge deck $L/2$) for detection, the detection object for the left and right width of the $L/4$, $3L/4$, 4 points, the main tower tower top of the A side of the tower $3^{\#}$, $4^{\#}$ point as a transfer point (from $3^{\#}$ station led to the top of the tower) The main cable measurement points on the left and right sides of the span are measured by infrared rangefinder (because the main cable measurement points in the span will be blocked by vehicles during the loading process of condition 1), and the specific measurement method is as follows: use a plumb line (hanging weight) to lower the main cable from the middle of the span (point A) to determine the corresponding plumb point on the main girder (point B), and measure the distance between the two points of each loaded position *AB* during the test of condition 1 to obtain the relative displacement of the main cable and the main girder for each loaded position. Relative displacement of the main cable and the main beam. The longitudinal deviation of the tower top is detected by station $3^{\#}$, which is set up on the left side of bank A (at the waste harbor about 100 m from the bridge), and the longitudinal deviation measurement points of the tower top are $1^{\#}$ and $2^{\#}$ (for condition 1 test). Layout of loading vehicles for condition 1 is shown in Figure 7.

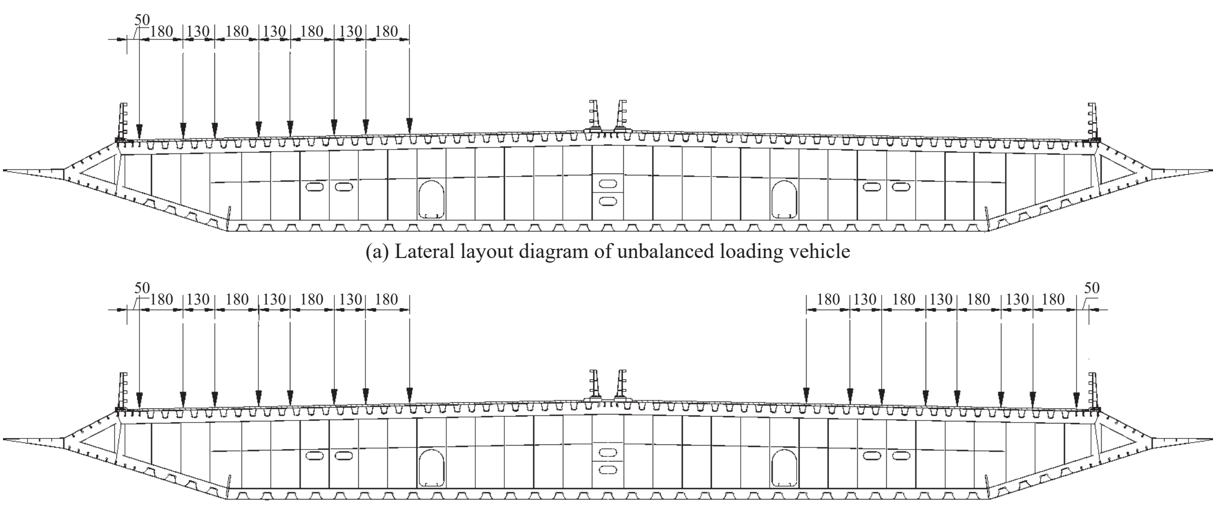

(a) Lateral layout diagram of unbalanced loading vehicle

(b) Symmetrical loading vehicle lateral layout diagram

Fig. 7 Lateral layout of loading vehicles (unit: cm)

3.2.3 Loading method of static load test

Case 1-Case 5 symmetrical loading were used 120, 80, 112, 88, 56 vehicles weighing about 350 kN load; Case 1-Case 5 partial load were used 60, 40, 56, 44, 28 vehicles weighing about 350 kN load, are divided into 2 levels of loading and 1 level of unloading. In order to save vehicle classes and facilitate the implementation of the program on-site, the partial load conditions for the symmetrical loading of the first level and the second level of loading[20], that is, the symmetrical loading of the second level of loading for the partial load of the full load. The lateral layout of vehicle loading position for each condition is shown in Figure 8. The loading process is based on 8 loading vehicles as a batch, and the spacing of loading vehicles in traveling is not less than 50 m. After 8 loading vehicles are parked in place, then the waiting loading area is notified to start the loading vehicles.

3.2.4 Specific loading time of static load test

The specific loading time of static load test is shown in Table 2.

3.3 Dynamic load test

The dynamic load test tests the response of the bridge under dynamic loading and analyzes the modal parameters such as frequency and vibration pattern of the bridge[21]. Based on the modal parameters, the load carrying capacity of the bridge is evaluated. According to

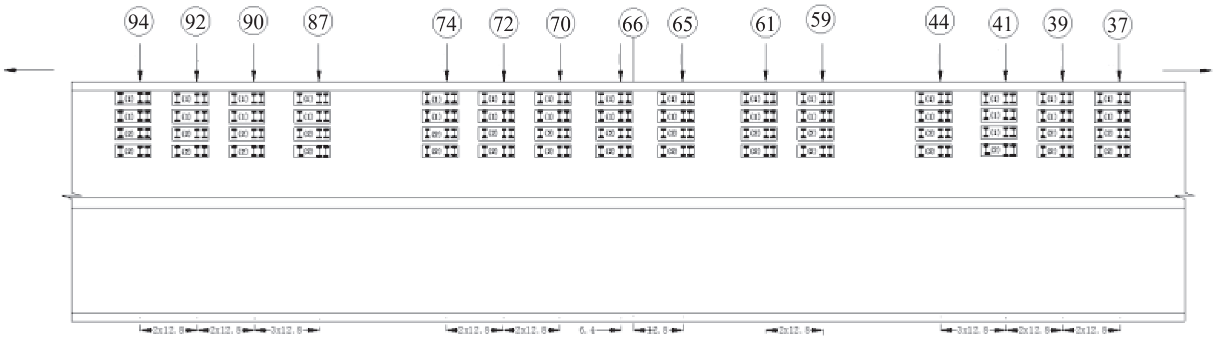

(a) Longitudinal layout diagram of unbalanced loading vehicle

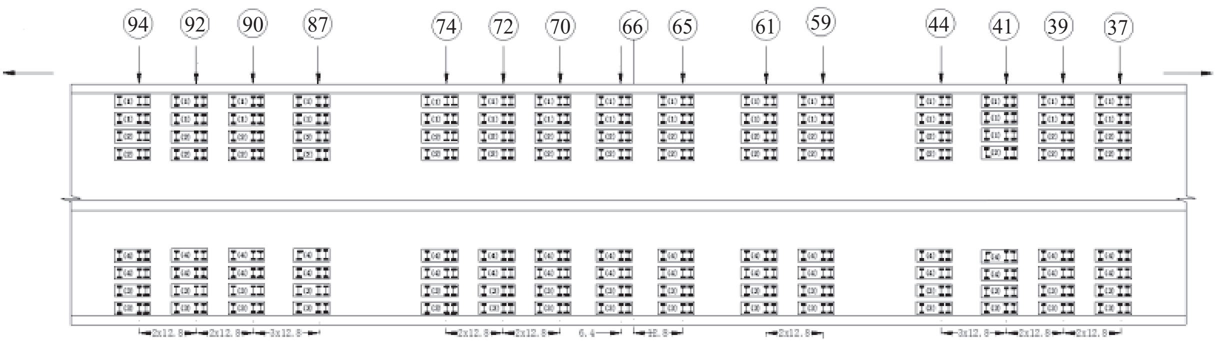

(b) Longitudinal layout diagram of symmetrical loading vehicle

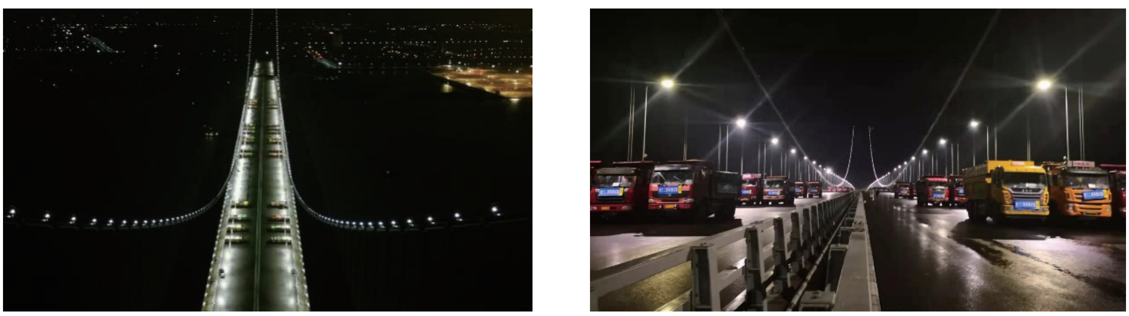

(c) Actual situation of load test site

Fig. 8 Layout of loading vehicles for condition 1

Table 2 Specific loading time nodes for static load test

Date	Before loading	Primary loading	Secondary loading	Third-stage loading	Fourth level loading	First level unloading	Secondary offloading
March 5	21:22	21:57	23:08	1:10+1 day	1:55	3:00	4:55
March 6	21:35	22:14	23:30	0:25+1 day	0:45	2:00	2:45
March 7	20:57	21:58	22:50	23:50	0:51+1 day	1:53	2:39
March 8	21:08	21:57	22:40	23:20	0:12+1 day	1:46	2:53
March 9	22:43	23:41	0:27+1 day	1:40	2:32	4:04	5:00

the specification, the suspension bridge needs to measure the first nine orders of the formation, and the results of the theoretical calculation of the first nine orders of the vibration mode of the Nizhou Waterway Bridge are shown in Table 3.

Table 3 The first nine orders of vibration pattern of Nizhou waterway bridge

No.	Description of vibration pattern	Self-oscillation frequency (Hz)
1	Main beam transverse bending	0.050 2
2	First-order anti-symmetric vertical bending of main beam	0.076 6
3	First-order symmetric vertical bending of main girder	0.101 5
4	Second-order anti-symmetric vertical bending of main beam	0.118 7
5	Second-order transverse bending of main beam	0.122 8
6	Second-order symmetric vertical bending of main girder	0.132 5
7	Third-order anti-symmetric vertical bending of main beam	0.174 4
8	Third-order symmetric vertical bending of main girder	0.176 7
9	Main cable transverse bending	0.200 9

The main girder measurement points are arranged in the side span 4 points and the middle span 16 points, the main cable measurement points are arranged in the middle span 4 points above the main cable, the main tower measurement points are arranged in the A-side, Dongguan side of the main tower on the crossbeam platform, the use of 8 sets of 3 062 T data acquisition instrument + 14 vertical 991B (2 standby, a total of 16, you need to borrow 4 from the ChengAn inspection) + 8 horizontal 991B (2 standby, a total of 10, you need to borrow 2 from ChengAn inspection), during the inspection process using GPS time synchronization measurement (do not use WiFi), the inspection process using GPS time synchronization measurement (do not use WiFi). (2 spare, a total of 10, need to borrow 2 from the Chengan test), the detection process using GPS time synchronization measurements (do not use WiFi). The specific measurement point arrangement is shown in Figure 9.

In the absence of any obstacles on the bridge deck, two loaded vehicles weighing about 400 kN were utilized to drive in parallel on the bridge deck at different speeds ranging from about 10 to 60 km/h in order to test the dynamic response of the structure under the action of travelling loads. By measuring the dynamic strain of the main girder mid-span $L/4$ and mid-span cross-section, the corresponding dynamic coefficients are obtained from the analysis. The specific arrangement of measurement points is shown in Figure 10. Two dynamic strain testing systems (EDX-100A-1H) and four dynamic strain transducers (KM-100B) were used, and the vehicles were two 400 kN loading trucks and two 3.5 m long, 30.0 cm wide and 5.0 cm high bow plates. First do the middle span $L/4$ section, and then do the middle span running jump car test.

3.4 Measuring point arrangement of structural health monitoring system

This paper mainly analyzes the monitoring data of the structural health monitoring system during the load-

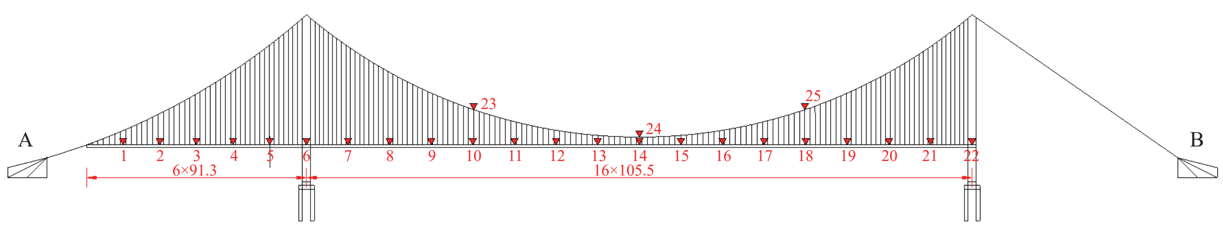

Fig. 9 Arrangement of pulsation measurement points (unit: cm)

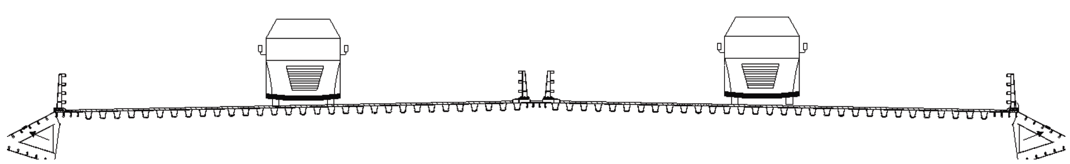

Fig. 10 Layout of measurement points for running test

ing test and compares them with the results of the on-site loading test[22]. The structural health monitoring system lists the arrangement diagrams of displacement, strain and vibration measurement points at the response location.

4 Data analysis

4.1 Strain data analysis of main girder under load test

The field static load test involved five working conditions. Among them, Case 1 (March 9) and Case 2 (March 6) were applied at the mid-span and $L/4$ of the Guangzhou side. The structural health monitoring system was arranged with strain gauges at these two control sections. Therefore these two working conditions are most favorable for testing whether the arranged strain gauges are normal or not, the variation of strain time history is shown in Figuer 11.

The specific values of the test results are shown in Table 4.

Strain data analysis results are: (1) sensor data ob-

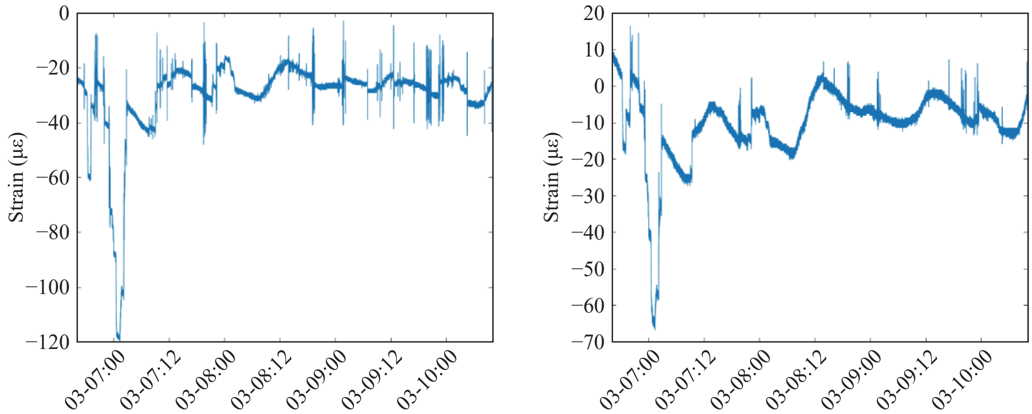

Fig. 11 Time course of strain at some measurement points

Table 4 Test result values

Strain Gauge No.		Initial value before loading	Fully loaded value	Residual value after unloading	Relative amount of residual deformation
	1	−37.9	−62.7	−46.4	0.34
	2	−40.4	−65.4	−50.4	0.40
	3	−32.8	−58.2	−41.7	0.35
	6	0	−66.4	−15	0.23
Working condition I	7	−26.4	−118.2	−32.7	0.07
	11	−41.5	−70.5	−53	0.40
	14	−23.1	−161.3	−36.4	0.10
	15 −40.8	−40.8	−74.4	0.10 15 −40.8	0.39
	16	−40.1	0.39 16 −40.1	−54.2	0.36
	1	−62.1	−76.8	−66.6	0.31
	2	−60.5	−81.3	0.31 2 −60.5 −81.3	0.20
	0.20	−55.2	−87.9	−61.2	0.18
Working Condition II	4	−53.6	−87.7	−66.6	0.38
	10	−58.6	−82.2	−64.2	0.24
	15	−50.4	−84.7	−59.1	0.25
	16	−16.3	−78.9	−30.8	0.23

Note: Residual deformation = (unloaded value-initial value) / (full load value-initial value)[23] tained during the load test to monitor the obvious graded loading and unloading situation; (2) strain data graded loading and unloading situation is obvious, unloaded residual deformation is small; (3) observation of the strain gauge monitoring data, monitoring data, local burrs are particularly large, for the burr amplitude of a small point, may be the vehicle loaded and unloaded through the location near the resulting local deformation, may also be the interference signal (noise); (4) the strain gauge monitoring data, monitoring data local burrs especially much, for burrs amplitude small points, may be the vehicle loaded and unloaded through the location near the generated For the point with small burr amplitude, it may be the local deformation generated near the position when the vehicle was loaded and unloaded, or it may be the interference signal (noise); (5) For the point with large burr amplitude, the reason may be the local large deformation generated near the position when the vehicle was loaded and unloaded.

4.2 Analysis of load test main beam deflection data

The deflection time history of some measuring points is shown in Figure 12, the monitoring results are shown in Tables 5 and 6, and the results show that: (1) the results of on-site testing and monitoring system GPS are basically the same, and the reason for a little error is that there is a difference between the GPS measurement points and the deployment points of the total station during the on-site testing; (2) when the most unfavorable loads (vehicular load) are arranged in the middle of the side spans and in the middle of the main span cross-section respectively, the corresponding deformation of the side spans and middle of the main spans are the largest, and the deformation at this position of the main cable is also the largest, and the main cable has the largest deformation. The deformation at the location is also the largest, and the vertical deformation of the main cable is basically the same as that of the corresponding bridge deck. This shows that the elastic deformation produced by the corresponding cables is particularly small; (3) GPS monitoring results can accurately reflect the loading and unloading of the load test, the overall operation of the GPS system is good; (4) the bridge main span is 1 688 m, the monitoring results show that the maximum deformation of the cross-section is 1.487 7 m, which is less

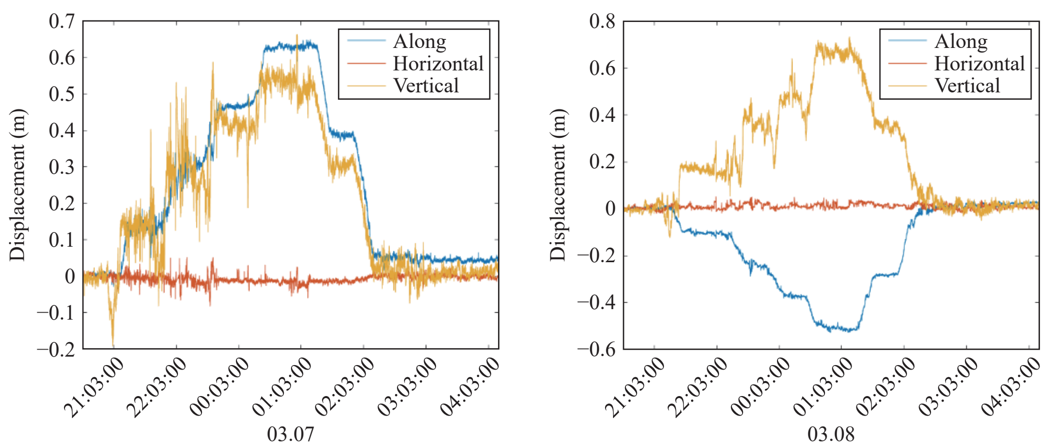

Fig. 12 Deflection at some measurement points program

Table 5 Relative value of GPS data (unit: m)

Item	Working condition I (maximum vertical displacement of main beam at mid-span)	Case I (tower top deflection)	Case II (maximum vertical displacement of side span main girder)	Case V (maximum vertical displacement of side span mid-span)
On-site Inspection Measurement	−1.02	0.34	−1.43	−0.89
Monitoring system GPS	−0.998 7	0.356 2	−1.487 7	−0.939 6
Difference	0.021 3	0.016 2	−0.057 7	−0.049 6
Relative Error	0.71%	4.76%	1.68%	2.62%

Table 6 Analysis of GPS results of the monitoring system (unit: m)

Item	Condition 1 (Maximum vertical displacement of main girder at mid-span)	Working condition I (tower top deflection)	Case II (Maximum vertical displacement of main girder at side span)	Case V (Maximum vertical displacement at mid-span)
Monitoring system GPS full load value	−0.998 7	0.356 2	−1.487 7	−0.939 6
Residual value	−0.01	−0.01	−0.021	−0.05
Elasticity value	−0.998 7	0.356 2	−1.487 7	−0.939 6
Theoretical model calculated value	−1.36	0.36 36	−1.81	−1.01
Calibration coefficient	0.898	0.98	0.92	0.96
Residual deformation coefficient	0.003	0.03	0.006	0.026

than the limit value of the deflection $L/400$, and it meets the specification design requirements; (5) analyzing GPS monitoring results, the calibration coefficient and the residual value are the same as those of the bridge deck. monitoring results, the calibration coefficient and residual deformation are within a reasonable range, indicating that the structural performance is better, the bearing capacity has a certain affluence, and the relative residual variance of the main control points are less than 0.2, indicating that the structure is closer to the elastic working state.

Due to the possibility of external interference during the measurement of deflection and strain by system instruments, noise may be generated, which can affect the accuracy of relevant data. In this paper, data processing techniques such as sliding average filtering and elimination of outliers are used to improve data quality and accuracy before data use.

4.3 Data analysis of modal parameters of main beam in load test

The spectral method was used to identify the modal parameters, using the finite element analysis software Midas[24]. The 3D model of the bridge is shown in Figure 13, the peak picking point as shown in Figure 14, and the first five orders of vibration shapes and frequencies identified based on each day's load test monitoring data are are shown in Tables 7 and 8 (only the main bridge tower and bridge deck are plotted in the simplified model).

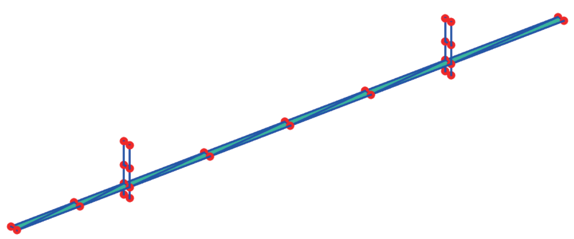

Fig. 13 Three-dimensional model of the bridge

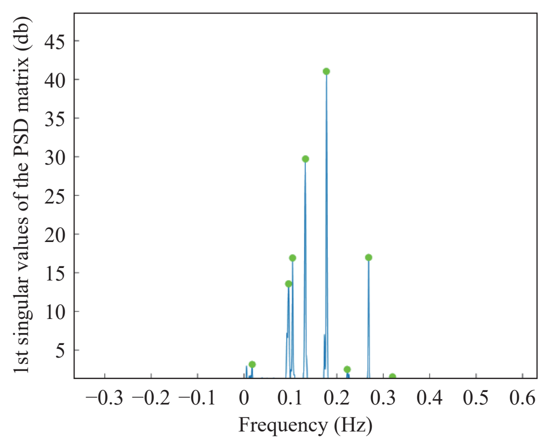

Fig. 14 Peak pickup points

Table 7 Frequency identification results

	First order	Second order	Third order	Fourth order	Fifth order
Monitoring Result	0.015	**0.096**	**0.104 6**	**0.132**	**0.178**
Load test result	0.056	**0.095**	**0.104**	**0.119**	**0.140**
Theoretical calculation results	0.05	**0.077**	**0.102**	**0.119**	**0.123**

Table 8 Comparison of results

	First order	Second order	Third order	Fourth order	Fifth order
Monitoring Result	0.015	**0.096**	**0.104 6**	**0.132**	**0.178**
Load test result	0.056	**0.095**	**0.104**	**0.119**	**0.140**
Theoretical calculation results	0.05	**0.077**	**0.102**	**0.119**	**0.123**

5 Conclusion

In this paper, for a large-span suspension bridge girder field loading static load and dynamic load test, and combined with the existing health monitoring system data on the bridge for comparative analysis, specifically analyzed the strain value of the main girder loaded case, GPS deflection value and the vibration data of the bridge, and obtained the following main conclusions:

(1) The strain gauge and GPS results can observe the obvious loading and unloading situation, and the collected vibration data can also effectively analyze the modal parameters of the structure, which indicates that the whole health monitoring system works well and the collected data are reliable.

(2) The deflection calibration coefficient and relative residual coefficient meet the Load Test Regulations, and the reliable measured frequencies obtained from the analysis and calculation are greater than the theoretical calculated frequencies, indicating that the overall stiffness of the structure meets the design requirements, and the structural mechanical performance meets the regulations and design requirements.

(3) By comparing the evaluation methods of the field load test, the health monitoring data are analyzed and excavated to evaluate the bearing capacity of the bridge during the load test, and the test results can be used as a reference for the subsequent evaluation of the structural health monitoring system of the bridge as well as the operation of the bridge.

6 Research shortcomings and prospects

This article proves through relevant examples that both the load testing equipment and the health monitoring system can meet the specifications and design requirements, demonstrating the feasibility and effectiveness of the monitoring based state evaluation index system and evaluation method. Further exploration is needed to explore the connections between different monitoring data, comprehensively consider different monitoring data, and propose more comprehensive and complete evaluation indicators. The specific shortcomings and prospects are as follows:

(1) This article mainly focuses on the comparison between on-site load tests and health monitoring data of bridges, evaluating whether the health monitoring system is operating normally, and conducting preliminary mining and analysis of monitoring data. Further in-depth data mining can be carried out in the future.

(2) From the perspective of bridge force analysis, considering the relationship between strain monitoring data, GPS monitoring data, inclined cable monitoring acceleration data, and bridge deck acceleration sensor monitoring data, a comprehensive damage evaluation index is proposed based on various monitoring data.

(3) From the perspective of data analysis, consider data-driven methods such as deep learning algorithms to deeply mine various monitoring data and identify more meaningful evaluation indicators.

Declaration of competing interest

The authors have no competing interests to declare that are relevant to the content of this article.

References

[1] Sun, L.M., Zhang, Q.W. Large-span bridges and their health monitoring systems in China[C]//International Symposium on Integrated Life-cycle Design & Management of Infrastructure. 2007.

[2] Li, H., Ou, J.P. Design and implementation of health monitoring systems for cable-stayed bridges (Ⅱ): implementations[J]. China Civil Engineering Journal, 2006, 39(4): 45–53.

[3] Masood, M.A., Masood, N.K., Ullah, F.K. Bridge vibration energy harvesting for wireless IoT-based structural health monitoring systems: A review[J]. Journal of Intelligent Material Systems and Structures, 2023, 34(19): 2209–2239.

[4] Xu, J.F., Feng, Z.M., Li, H.W., et al. Study on vibration amplitude and force identification of cables of cable-stayed bridge based on dynamic monitoring[J]. Journal of Highway and Transportation Research and Development , 2022, 39(2): 111–116.

[5] Lakshmi, K., Apte, P. A damage detection technique using bridge influence surfaces for structural health monitoring of bridges[J]. Recent Trends in Civil Engineering, 2022, 274: 865–874.

[6] Wang, C., Zhong, J.W., Zhu, H.P. Fatigue assessment of steel box girder based on measured stress of health monitoring system[J]. Journal of Wuhan University of Science and Technology, 2012, 34(12): 103–107.

[7] Xu, J.L., Dong, Y.K., Zhang, Z.H. Full scale strain monitoring of a suspension bridge using high performance

distributed fiber optic sensors[J]. Measurement Science and Technology, 2016, 27(12): 124017.

[8] Wei, S.Y., Zhang, Z.H., Li, S.L., et al. Strain features and condition assessment of orthotropic steel deck cable-supported bridges subjected to vehicle loads by using dense FBG strain sensors[J]. Smart Materials and Structures, 2017, 26(10):

[9] Li, C.X., Li, Y., Chen, Z.Y., et al. Fatigue characteristics of steel box girder diaphragm based on measured traffic flow[J]. Journal of Chang'an University (Natural Science Edition), 2019, 39(5): 48–58.

[10] Belmokhtar, M., Schmidt, F., Chevalier, C., et al. Vibration-Based Method for Structural Health Monitoring of a Bridge Pier Subjected to Environmental Loads[J]. Experimental Vibration Analysis for Civil Engineering Structures, 2022, 224: 73–82.

[11] Shi, X.W., Wang, K.M., Jiang, J., et al. Study on loading efficiency of bridge load test based on old and new design codes[J]. GongluJiaoTongKeJI, 2012, 8(9): 263–266.

[12] Saroufim, A., Issa, M.A., Issa, M.A. Optimized finite element analysis and strengthening assessment of the I-39 Kishwaukee bridge utilizing proof load testing[J]. Journal of Civil Structural Health Monitoring, 2024, 14(3): 545–574.

[13] Nugroho, U., Wardani, S.P.R., Setiadji, B.H. Rigid pavement acceleration-velocity dynamic behavior induced by traffic load[J]. Civil Engineering and Architecture, 2024, 12(3): 1386–1394.

[14] Zhang, K.X., Qi, T.Y., Li, D.C., et al. Health Monitoring-Based Assessment of Reinforcement with Prestressed Steel Strand for Cable-Stayed Bridge[J]. Structural Durability & Health Monitoring, 2022, 16(1): 53–80.

[15] Mohammad, A., Antonio, N., Nafiseh, K., et al. Bridge load testing and damage evaluation using model updating method[J]. Engineering Structures, 2022, 252.

[16] Wang, G.H., Hu, L.H. Study on damage identification of bridge structure based on the method of element modal strain energy[J]. Journal of the China Railway Society, 2006, 28(3): 83–86.

[17] He, M.L., Song, J., Lin, H.L., et al. Multi-lane vehicle load and deflection response characteristics of long-span highway bridge[J]. Journal of Highway and Transportation Research and Development, 2022, 39(S2): 76–81,141.

[18] Cherid, D., Bourahla, N., Laghoub, S.M., et al. Sensor number and placement optimization for detection and localization of damage in a suspension bridge using a hybrid ANN-PCA reduced FRF method[J]. International Journal of Structural Integrity, 2021, 13(1): 133–149.

[19] Fu, W., Liu, B. Analysis of the Application of Static Load Test in Bridge Bearing Capacity Testing[J]. Journal of Architectural Research and Development, 2024, 8(3): 36–41.

[20] Győző, K., László, Á.S., István, P., et al. Different conical angle connection of implant and abutment behavior: A static and dynamic load test and finite element analysis study[J]. Materials, 2023, 16(5): 1988–1988.

[21] Wang, H.Q., Nagayama, T. Response spectrum model of vehicle dynamic load for the prediction of bridge vibration level due to single vehicle-passage[J]. Engineering Structures, 2022, 260: 114180-.

[22] Yang, Z.K., Yang, Y.X., Yu, H.B. Study on optimal sensor arrangement on bridge structure based on sensitivity and effective independence method[J]. Journal of Highway and Transportation Research and Development, 2022, 39(4): 83–92.

[23] Huang, G.P., Hu, J.H., Cui, J.F., et al. Study on girder end displacement characteristics of steel truss suspension bridge based on measurement data[J]. Journal of Highway and Transportation Research and Development, 2022, 39(5): 65–73.

[24] Alessandra, A.D., Rosaria, M.P. Model assessment of a bridge by load and dynamic tests[J]. Engineering Structures, 2023, 275(PA):